Detonation Development in Hydrogen/air Mixtures inside a Closed Chamber: Role of a Cold Wall

Haiyue Li*, Zheng Chen

CCSE, CAPT, SKLTCS, College of Engineering, Peking University, Beijing 100871, China

Abstract

Detonation development from a hot spot has been extensively studied, where ignition occurs earlier than that in the surrounding mixtures. It has also been reported that a cool spot can induce detonation for large hydrocarbon fuels with Negative Temperature Coefficient (NTC) behavior, since ignition could happen earlier at lower temperatures. In this work we find that even for hydrogen/air mixtures without NTC behavior, a cold wall can still initiate and promote detonation. End-wall reflection of the pressure wave and wall heat loss introduce an exothermic center outside the boundary layer, and then autoignitive reaction fronts on both sides may evolve into detonation. The right branch is further strengthened by large temperature gradient near the cold wall, and exhibits different dynamics at various initial conditions. Small excitation time and large diffusivity of hydrogen provide the possibility for detonation development within the limited space between the autoignition kernel and the cold wall. Moreover, detonation may also develop near the flame front, which may or may not co-exist with detonation waves from the cold wall. Correspondingly, wall heat flux evolution exhibits different responses to detailed dynamic structures. Finally, we propose a regime diagram describing different combustion modes including normal flame, autoignition, and detonation from the wall and/or the reaction front. The boundary of normal flame regime qualitatively agrees with the prediction by the Livengood-Wu Integral method, while the detonation development from both wall and reaction front observes Zel'dovich mechanism. Compared to hydrocarbons, hydrogen is resistant to knock onset but it is more prone to superknock development. The latter mode becomes more destructive in the presence of wall heat loss. This study isolates and identifies the role of wall heat loss on a potential mechanism for superknock development in hydrogen-fueled spark-ignition engines.

Keywords: Detonation development; End wall reflection; Isothermal cold wall; Wall heat flux; Hydrogen

*Corresponding author.

Email address: lihaiyue@pku.edu.cn (Haiyue Li)

1. Introduction

Being carbon free, hydrogen is a promising alternative fuel for spark-ignition engines (SIEs) under increasing environmental concerns [1-3]. In the highly boosted SIEs fueled by hydrogen, the extremely destructive superknock may occur due to large energy density in unburnt mixtures. It is universally acknowledged that superknock is closely related to detonation development [4, 5]. Therefore, it is necessary to understand the mechanism for detonation development under engine-relevant conditions. To this end, extensive studies have been conducted. According to Zel'dovich [6, 7] and SWACER (shock-wave amplification by coherent energy release) mechanism of Lee et al. [8, 9], detonation development is observed under certain temperature or/and concentration non-uniformity in unburnt mixtures. In the literature detonation development from a hot spot has been extensively studied. For example, Bradley and coworkers [10, 11] identified different modes of reaction front and proposed a detonation peninsula. Kurtz and Regele [12] analyzed different time scales involved in the detonation development.

In most combustion engines wall heat loss is omniscient, while detonation development from a cool spot is comparably less studied. For large hydrocarbon fuels with the Negative Temperature Coefficient (NTC) behavior, ignition may occur earlier inside the cool spot compared to that in the surrounding mixtures, and as such detonation development can also be triggered by the Zel'dovich mechanism [13]. However, this mechanism does not apply to fuels without NTC behavior. For hydrogen combustion, ignition enhancement by the cold boundary through Ludwig–Soret diffusion has been reported in [14], whereas the transition to detonation has not been observed. It is still not clear whether wall heat loss can help the detonation initiation for fuels without NTC behaviors.

In addition to thermal and concentration non-uniformity in unburnt mixtures, we further note that end-wall reflection of pressure waves may also causes detonation development from the wall. Near-wall detonation development is observed in some studies conducted in the absence of wall heat loss [15-18]. Liberman et al. [15] observed the near-wall detonation development caused by the flame-induced acoustic wave. Yu et al. [16] found that even in 1D flow only with an initial propagating flame detonation can still develop when the reactivity of the end-gas is sufficiently high. Dai et al. [18] investigated the effects of end-wall reflection on autoignition and detonation development from local temperature non-uniformity. Furthermore, the wall heat loss is frequently observed to suppress such detonation development. For example, Terashima et al. [19] found that the knocking intensity for n-heptane/air mixtures peaks at the NTC region, which is greatly reduced by the wall heat loss. Sow et. al [20] studied detonation onset in a thermally stratified constant volume reactor, and identified different detonation mode for positive and negative the bulk-gas temperature gradient. Wang et al. [21] and Han et al. [22] studied the effect of heat loss boundary on deflagration-to-detonation transition in narrow channels. They observed that heat loss reduces the flame acceleration rate and delays the occurrence of DDT. Wu and Wang [23] experimentally studied the effect of wall heat exchange on DDT. They found that heat loss reduces flame acceleration rate and leads to quenching detonation.

Recognizing the paucity on detonation initiation and promotion from the cold wall for fuels without NTC behaviors, this study aims to numerically examine the role of wall heat loss in detonation development for hydrogen/air mixtures inside a closed chamber. Potential detonation modes under engine-relevant conditions are identified and discussed. The remainder of this paper proceeds as follows. Section 2 describes the numerical model and methods. Section 3 discusses the multiple dynamics involved during the detonation development under an isothermal wall boundary condition, as well as the resulting extremely strong pressure wave and wall heat flux oscillations. Section 4 presents the conclusions.

2. Numerical model and methods

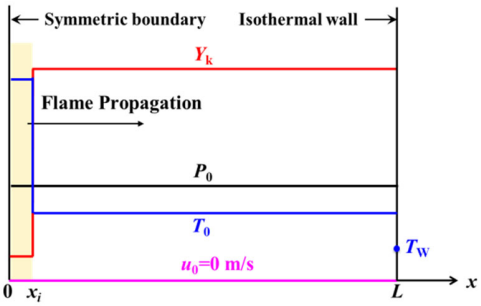

Fig. 1. Initial and boundary conditions used in the simulation of flame propagation and quenching

We consider detonation development during a 1D premixed flame propagating inside a closed chamber with an isothermal cold wall. The initial and boundary conditions are shown in Fig. 1. The computational domain is $0 \le x \le L$, and the chamber length is fixed to be $L = 2$ cm. The propagating flame is initialized by a hot kernel containing burned gas at adiabatic flame temperature on the left side ($0 \le x \le x_i = 0.1$ mm). Initially, the flow speed is zero (i.e., $u = 0$) everywhere and the initial pressure, P_0, is uniformly distributed inside the computational domain. The initial temperature of unburned gas, T_0, is uniformly distributed outside the hot kernel (i.e., $x_i \le x \le L$). The wall at $x = L$ is isothermal and chemically inert, with a fixed temperature at $T_w = 450$ K in the present study.

The transient flame propagation and autoignition processes are simulated by the in-house code A-SURF [13, 24, 25]. A-SURF solves the conservation equations for compressible, multi-component, reactive flow using the finite volume method. The detailed hydrogen chemistry developed by Li et al. [26] is used. CHEMKIN packages [27] are incorporated into A-SURF to calculate the thermal and transport properties as well as the reaction rates. A dynamically adaptive mesh is used to accurately and efficiently resolve the propagating flame front and detonation. The reaction zone is always fully covered by the finest mesh with a size of 0.8 μm. To achieve a better resolution on the wall heat flux, a smaller mesh size of 0.05 μm is used at the isothermal wall. The corresponding time step is 3.9×10^{-11} s and thereby the Courant Friedrichs-Lewy (CFL) number is always equal or less than 0.25. The mixture-averaged model is used and the Soret diffusion of H_2 and H is included in simulations. A-SURF has been shown to be able to accurately simulate ignition, flame propagation and detonation development in previous studies [13, 24, 25]. The details on governing equations and numerical methods used in A-SURF can be found in the Supplementary Document of [13, 24] and thereby are not repeated here. The numerical treatment of isothermal boundary condition and grid dependence study are shown in the Supplementary Material.

3. Results and discussions

Table 1 cases considered in the simulation

Case	(T_0, P_0)	observations
1	(1000 K, 5 atm)	W: shock, ignition kernel
2	(1000 K, 10 atm)	W: shock, no ignition kernel
3	(900 K, 20 atm)	W: detonation in the right branch
4	(1100 K, 10 atm)	F+W: double detonation waves
5	(1150 K, 5 atm)	F: no end-gas autoignition
6	(1150 K, 8 atm)	F: end-gas autoignition

W and F respectively denote to the detonation modes where detonation respectively develops *near the wall* and *near the flame front*

Demonstrative cases in the present work are summarized in Table 1. First, we illustrate the dynamic behaviors during detonation development from the cold wall by case 1 (T_0 = 1000 K and P_0 = 5 atm), cases 2 (T_0 = 1000 K and P_0 = 10 atm) and case 3 (T_0 = 900 K and P_0 = 20 atm). In case 1 and case 2, detonation is fully developed in the left branch. Meanwhile, the pressure (shock) wave and heat release are not fully coupled into a detonation in the right branch, and the formation of the post-shock autoignition kernel is respectively observed in case 1 and not observed in case 2. In case 3 only the right branch of detonation develops, where the shock wave and reaction front are tightly coupled before reaching the wall.

Then we consider detonation from the reaction front by case 4 (T_0 = 1100 K, P_0 = 10 atm), case 5 (T_0 = 1150 K, P_0 = 5 atm), and case 6 (T_0 = 1150 K, P_0 = 8 atm). In case 4 wall-induced detonation co-exist with the detonation from the flame front. In case 5 autoignition occurs in the end-gas without the transition to detonation. In case 6 neither autoignition nor detonation is observed in the unburnt mixtures.

Finally, we propose and interpret a regime diagram on potential combustion modes.

3.1 Detonation developing from the cold wall

We first examine how detonation develops from a cold isothermal wall. Case 1 (T_0 = 1000 K and P_0 = 5 atm) is chosen to illustrate the involved dynamics. In the corresponding case with an adiabatic wall, the combustion mode is similar to that for case 7 in [16], i.e. an leftward propagating detonation develops from the adiabatic wall due to the end-wall reflection of pressure waves. However, in case 1 of the present study with an isothermal wall, double reaction fronts propagate towards opposite directions with different dynamic behaviors.

The temporal evolution of temperature, pressure, and heat release rate distributions for case 1 is shown in Fig. 2. It is seen that, a local autoignition kernel forms (line #3) at x = 1.9 cm around t = 258 μs. Compared to the adiabatic case, the near-wall region in case 1 remains unburnt since the wall heat loss greatly inhibits the autoignition inside the boundary layer on the wall. Then both heat release rate and pressure rapidly build up in this exothermic center, resulting in two reaction fronts propagating towards opposite directions (line #4). The autoignition front propagating leftwards then evolves into a detonation (lines #5 and #6), and finally recedes into a strong shock wave after its collision with the rightwards propagating flame (line #7). Meanwhile, the autoignition front propagating rightwards does not evolve into a fully-developed detonation since there is not enough space/reactant between the autoignition kernel and end wall. Nevertheless, a weak shock wave forms during the end-wall reflection.

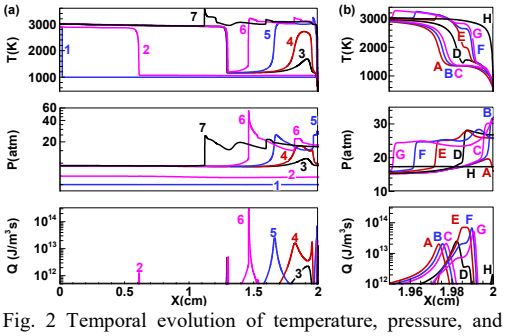

Fig. 2 Temporal evolution of temperature, pressure, and heat release rate distributions for case 1 in the whole domain (a) and in the near-wall region (b). The time sequence from line #1 to #7 is: 0, 117.19, 257.97, 258.28,

259.06, 260.20, and 261.95 μs. The time sequence from lines #A to #H is: 258.67, 258.71, 258.75, 258.87, 258.98, 259.06, 259.14, and 266.02 μs.

Similar behaviors on autoignition and detonation development are experimentally observed using rapid compression machine (RCM) in [28, 29]. However, it is difficult to resolve the corresponding near-wall dynamics by optic methods. In the present simulation work, Figure 2(b) shows details on the interaction between the rightwards propagating autoignition front and the end wall. The time for line #A in Fig. 2(b) is t = 258.67 μs, which is immediately after line #4 in Fig. 2(a) at t = 258.28 μs. The pressure wave propagates faster and reaches the wall earlier than the reaction front (see line #A in Fig. 2b). When the pressure wave reflects on the wall, it is intensified and evolves into a shock wave (line #B). The shock compression induces another autoignition in the unburnt mixture around x = 1.99 mm (lines #D and #E). This autoignition generates a new pressure wave propagating rightwards (line #F) and then reflecting on the wall (line #G). At this moment, the reaction front is still left behind at some distance from the wall and later it reaches the wall (line #H).

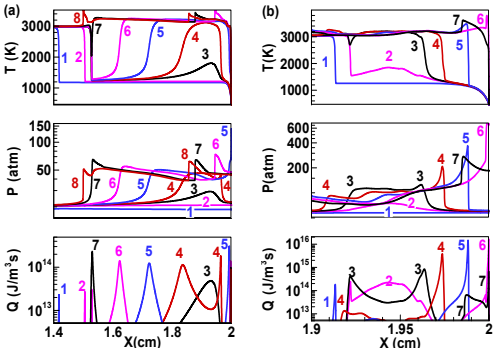

Fig. 3. Temporal evolution of temperature, pressure, and heat release rate distributions for (a) case 2 and (b) case 3. The time sequence from line #1 to #8 in (a) is: 304.69, 320.31, 326.56, 326.72, 327.03, 327.42, 327.89, and 328.05 μs. The time sequence from line #1 to #7 in (b) is: 369.14, 392.58, 393.98, 394.14, 394.69, 394.84, and 404.30 μs.

The extent of detonation development strongly depends on the initial temperature and pressure. The dynamics are demonstrated by cases 2 (T_0 = 1000 K and P_0 = 10 atm) and case 3 (T_0 = 900 K and P_0 = 20 atm) with increasing energy density in unburnt mixtures. Results are shown in Fig. 3. For case 2, the rightwards propagating pressure wave evolves into a shock wave before reaching the wall (see lines #4 and #5 in Fig. 3a). Meanwhile, the reaction front has entered the thermal boundary layer on the wall and thereby there is no autoignitive reactant adjacent to the original reaction zone. In case 3, the rightwards propagating autoignition front also evolves into a detonation (see lines #4 and #5 in Fig. 3b), whereas the leftwards propagating branch has inadequate space to fully develop into a detonation. Particularly, although in case 3 the location for detonation development is also near the reaction front, we still delineate such case to the near-wall type since no detonation occurs in the corresponding case with adiabatic wall (See the third part of the Supplementary Material).

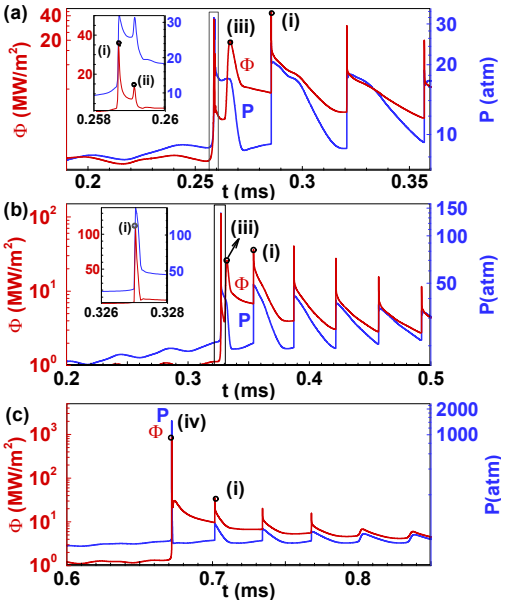

Fig. 4. Temporal evolution of wall heat flux and pressure on the wall for (a) case 1, (b) case 2, and (c) case 3. The marked local maxima correspond to wall interactions with (i) shock wave, (ii) pressure wave, (iii) reaction front, and (iv) detonation, respectively.

It is well known that superknock is characterized by extremely high and destructive pressure oscillations [4, 30, 31]. However, there is little work on the extremely large wall heat flux, which potentially triggers thermal fatigue and reduces the lifetime of combustion engines [32, 33]. Temporal evolution of the pressure on the wall and wall heat flux for cases 1 to 3 are shown in Fig. 4. The wall heat flux is defined as the product of thermal conductivity of the gaseous mixture and temperature gradient on the wall, i.e. $\Phi = \lambda(\mathrm{d}T/\mathrm{d}x)$. It is noted that the wall heat flux decreases with mesh size when wall interactions with the shock wave is included (See the second part of the Supplementary Material). In case 1, wall interactions with developing shock (lines #A and #B in Fig. 2b), pressure wave generated by post-shock autoignition (line #G in Fig. 2b), reaction front (line #H in Fig. 2b) sequentially leads to the local maximum (i), (ii), and (iii) in Fig. 4(a). The remaining local maxima after (iii) on the Φ-t curve is introduced by the back-and-forth propagating shock wave degenerated from the

leftwards propagating detonation. This detonation branch is stronger and becomes the dominant one after consuming all reactants inside the confined space. In case 2, only one local maximum, (i), appears before thermal quenching, which corresponds to the rightwards propagating shock impinging on the wall. The following local maximum induced by pressure wave (ii) is not observed due to the absence of a post-shock autoignition kernel. In case 3 the local maxima introduced by the shock wave and reaction front merges into a maximum at a greater order in magnitude, since the shock wave and heat release are tightly coupled into a fully-developed detonation.

The cold wall is expected to reduce the combustion intensity for fuels without NTC behavior. However, the above results for cases 1 to 3 indicate that under engine-relevant conditions, cold wall introduces substantial thermal inhomogeneity and as such can facilitate the detonation development. The detonation development is closely related to superknock in SIEs, where very strong pressure oscillations and extremely high wall heat flux cause severe damage to engines as well as significant efficiency loss.

3.2 Detonation developing from reaction front

In previous studies in the absence of wall heat loss [16, 17], detonation development are observed from the end wall or the reaction front. In this subsection we examine the role of a cold wall in the latter mode.

Case 4 (T_0 = 1100 K, P_0 = 10 atm) is selected to demonstrate the hybrid mode where detonation develops from both the reaction front and the end wall. In the corresponding case with an adiabatic wall, the combustion mode is consistent with case 6 in [16], i.e., detonation only develops from the reaction front and autoignition occurs in the end-gas. In case 4 with an isothermal cold wall, an additional detonation wave is introduced by wall heat loss, and as such double detonation waves are observed inside the confined chamber.

The temporal evolution of temperature, pressure, and heat release rate distributions for case 4 is plotted in Fig. 5. It is seen that, a conventional flame (lines #1 and #2) evolves into a detonation (lines #3 and #4) at around t = 0.128 ms. Immediately afterwards, an autoignition kernel forms in the end-gas near the wall (line #5), resulting in two autoignition fronts propagating in the opposite directions. The leftwards propagating reaction front rapidly consumes remaining reactants trapped in the middle, while in the right branch a decoupled shock wave forms ahead of the reaction zone (line # 6) and reflects on the wall (line #7). After colliding with this reflected shock wave (line #8), the former shock wave propagating in mixtures undergoing autoignition interacts with the wall (line #9).

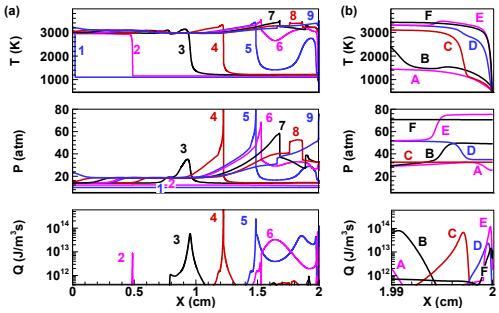

Fig. 5. Temporal evolution of temperature, pressure, and heat release rate distributions for case 4 (a) in the whole domain (b) in the near-wall region. The time sequence from lines #1 to #9 in (a) is: 0.00, 74.22, 127.97, 129.38, 130.70, 130.94, 131.88, 133.13, 134.14 μs. The time sequence from lines #A to #F in (b) is: 130.94, 131.02, 131.88, 134.06, 134.14, 134.45 μs.

Near-wall dynamics for case 4 are further described in Fig. 5(b). The weak shock evolving from the rightwards propagating autoignition approaches (line #A) and reflects on the wall (line #B). Shortly afterwards, the strong shock degenerated from the detonation formed near the reaction front also reaches (line #D) and reflects on the wall (line #E). Meanwhile, the decoupled reaction front moves towards the wall (lines #A to #E) and finally quenches (lines #F) after the second shock-wall interaction.

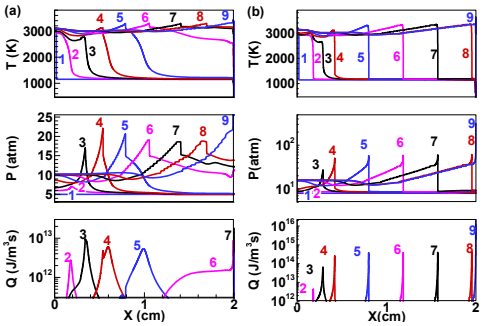

Fig. 6. Temporal evolution of temperature, pressure, and heat release rate distributions for (a) case 5 and (b) case 6. The time sequence from line #1 to #9 in (a) is: 0.00, 15.55, 16.72, 17.81, 19.22, 20.78, 22.97, 24.84, 27.11 μs. The time sequence from line #1 to #9 is: 0, 21.48, 24.02, 24.77, 26.72, 28.67, 30.62, 32.58, 32.81 μs.

We also note that such near-wall detonation does not always occur under other initial temperature and pressures. Case 5 (T_0 = 1150 K, P_0 = 5 atm) and case 6 (T_0 = 1150 K, P_0 = 8 atm) are selected to demonstrate potential combustion modes and results are shown in Fig. 6. In case 5, the normal propagating flame (lines #1 and #2 in Fig. 6a) transits into detonation (line #3) at around t = 0.015 ms. Immediately after that, the end-gas autoignition

occurs near the flame front and rapidly consumes the remaining reactants. Meanwhile, the heat release rate at the detonation front gradually decreases (lines #4-6), and then the degenerated shock wave continues to propagate rightwards (lines #7 and #8) and reflects on the wall (line #9). In case 6, the transition to detonation occurs at around t = 0.024 ms (lines #3 and #4 in Fig. 6b). This detonation continues to propagate rightwards (lines #5 to #8) and then collides with the wall (line #9). It is seen that no autoignition or detonation develops in the end gas in case 6. In corresponding cases with adiabatic wall, the same combustion modes are exhibited, indicating that a cold isothermal wall has little influence on the combustion mode if near-wall detonation is not initiated.

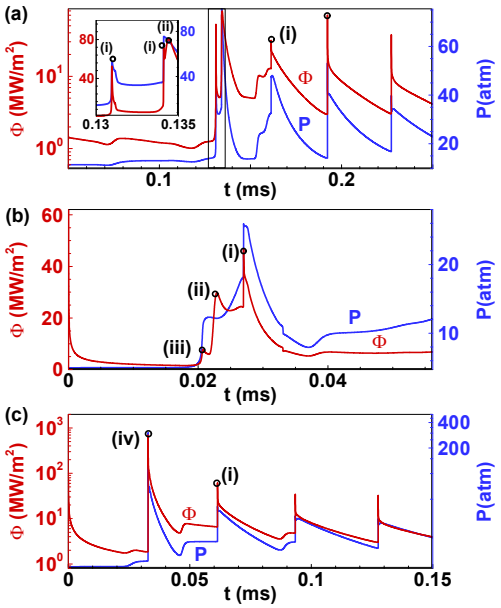

Fig. 7. Temporal evolution of wall heat flux and pressure on the wall for (a) case 4, (b) case 5, and (c) case 6. The marked local maxima of correspond to wall interactions with (i) shock wave, (ii) reaction front, (iii) pressure wave, and (iv) detonation.

Correspondingly, the temporal evolution of the pressure on the wall and wall heat flux for cases 4 to 6 is shown in Fig. 7. In case 4, double local maxima (denoted as the first and second #i in Fig. 7a) before thermal quenching (#ii in Fig. 7a and line #F in Fig. 5b) are observed. They are respectively induced by the sequential weak (lines #A and #B in Fig. 5b) and strong (lines #D and #E in Fig. 6b) wall interactions with the shock wave. In case 5, the pressure wave (line #6 in Fig. 6a), reaction front (line #7 in Fig. 6a) and subsequent shock wave (line #9 in Fig. 6a) sequentially interact with the wall, denoted by points (iii), (ii) and (i) in Fig. 7(b) respectively. In case 6, the direct collision between detonation and the wall leads to a maximum wall heat flux around 700 MW/m^2 (line #9 in Fig. 6b and #iv in Fig. 7c). After that only the shock wave propagates back-and-forth inside the closed chamber and causes a series of local maxima (#i in Fig. 7c) in descending order.

Usually end-gas autoignition and detonation development are expected to significantly increase the combustion intensity and cause destructive phenomena. However, the above results for cases 4 and 5 indicate that if the direct collision of detonation with the wall can be avoided, the wall heat flux can be greatly reduced. The results for cases 1-6 indicate that the detonation-wall interaction is the most destructive and has the highest wall heat flux. Fortunately, the extremely high wall heat flux does not frequently occur when detonation first develops near the reaction front since the autoignition of reactants close to the wall prohibits the detonation-wall interaction.

3.3 Regime diagram for combustion modes

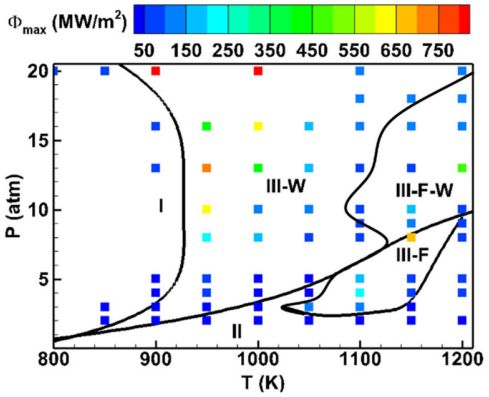

Fig. 8. Regime diagram of different combustion modes against the initial pressure and initial temperature, which are described in the text. The points represent different cases considered in simulations and the maximum wall heat flux for each case is reflected by its color.

Finally, a regime diagram, Fig. 8, describing different combustion modes in the plot of initial pressure vs. initial temperature, is obtained based on simulations for different thermal conditions. The regime boundaries are fitted by corresponding modes in simulation data. Similar to results in [16], three combustion modes are identified for end-gas combustion. Specifically: Regime I, normal combustion without autoignition and detonation development; Regime II, end-gas autoignition without detonation development; Regime III, detonation development. Based on the location a detonation wave develops, Regime III is further classified into III-W, III-F, and III-F-W, which respectively denotes detonation development from the wall, from the reaction front, and from both. The state (T_0=1200 K, P_0=13 atm) is an exception point in this diagram and is not otherwise specified. Its

combustion mode is similar to case 6 with (T_0=1150 K, P_0=8 atm) where only detonation develops from the reaction front and no abnormal combustion (i.e., autoignition and detonation) occurs in the end-gas.

In regime I normal combustion occurs without end-gas autoignition and detonation development. The boundary of regime I has similar shape with that with adiabatic walls (see Supplementary Material in [16]), and can also be qualitatively predicted by Livengood-Wu Integral method. Therefore, in the presence of the cold wall, the transition to abnormal combustion is mainly determined by the properties of bulk unburnt mixtures, and is minorly influenced the cold isothermal wall. The non-monotonic dependence on pressure correlates to the turning behavior of hydrogen-oxygen explosion limit. The three-body termination reaction $H+O_2$ (+M) = HO_2 (+M) renders the unburnt mixtures overall non-explosive at around 10 atm [34]. Consequently, hydrogen combustion is pretty resistant to knock onset, i.e., hydrogen autoignition happens around 800 to 950 K, whereas autoignition occurs at around 530 K in hydrocarbon-fueled gasoline engines [35].

As the initial temperature increases over the boundary of Regime I, abnormal combustion occurs. Specifically, at relatively low initial pressure end-gas autoignition occurs (Regime II), whereas at relatively high initial pressure detonation development is observed (Regime III). This is because at higher initial pressure the unburnt mixtures contain larger energy density and are thereby more prone to detonation development [7, 28, 36]. The boundary of Regime III-W (including III-F-W) denotes the transition in the near-wall combustion mode from end-gas autoignition to detonation development. As discussed in Section 3.1, detonation could develop from both side of the autoignition kernel formed near the wall. Compared to the left branch, the right branch is greatly enhanced by large temperature gradient on the wall via Zeldovich mechanism, and thereby is more frequently seen under various initial conditions. Therefore, the transition from regime II to regime III-W depends on detonation development of the right branch. At the time end-gas autoignition is about to occur, the near-wall temperature gradient varies from zero outside the finite thickness of the thermal boundary layer to very steep on the wall. Therefore, the pressure wave propagating at both low and high sound speed can be synchronized with the heat release, and transition to detonation occurs at a wide range of initial temperature.

In addition to proper temperature gradient, the detonation initiation from the cold wall is also subjected to the acoustic-to-excitation time ratio, $\varepsilon = x_s/(a\tau_e)$[31]. x_s is proportional to the thickness of the thermal boundary layer at the ignition delay time, τ_i. The larger diffusivity of hydrogen leads to a thicker boundary layer on the wall and hence introduces a larger x_s compared to that of hydrocarbons. Together with the shorter excitation time, τ_e, large acoustic-to-excitation time ratio allows the hydrogen detonation development in the very thin near-wall region. The characteristics for hydrogen combustion further explains why in hydrogen-fueled combustion engines extremely destructive superknock development is more likely to occur as long as the end-gas becomes autoignitive. It is also seen in Fig. 8 that detonation initiation from the cold wall occurs at higher pressure as the unburnt temperature increases. This is because at higher temperature the thickness of the thermal boundary layer, x_s, is smaller, whereas the sound speed, a, is larger. Therefore, detonation tends to develop at higher pressure, which is correlated to sufficiently high energy density and short excitation time.

The boundary of regime III-F (including III-F-W) denoting the detonation initiation from the reaction front can also be interpreted by the reactivity gradient during flame propagation. Unlike the deep temperature gradient on the wall, the thermal and species diffusion from the burnt zone to the preheated zone [16] introduces a shallow reactivity gradient near the flame front. Consequently, the reaction front is likely to couple with the pressure wave propagating at higher speed, and thereby corresponds to higher initial temperature. Moreover, a supersonic reaction front is generated via this mechanism above the upper bound, e.g., at (T_0 = 1200 K, P_0 = 5 atm). As mentioned in Section 3.2, detonation development from the reaction front is less influenced by the heat loss at the wall. However, the combustion mode is determined by the location (near the flame front, or near the wall) detonation first develops. The competition of detonation initiation time leads to a complex left boundary of the regime III-F (including III-F-W), and further increases the difficulty in accurate prediction and control the hydrogen combustion in engines.

The maximum wall heat flux, Φ_{max}, strongly depends on the combustion regime. We find that Φ_{max} is below 50 MW/m^2 in regime I and II, while it is usually in the order of $O(100)$ MW/m^2 in regime III. It is also noted that in regime III, Φ_{max} can further increase if a smaller mesh size is used. Extremely large Φ_{max} (over 700 MW/m^2) appears when the detonation directly collides with the wall, such as case 3 (T_0 = 900 K, P_0 = 20 atm) and case 6 (T_0 = 900 K, P_0 = 8 atm). Such extremely destructive detonation-wall interaction is more frequently observed in regime III-W when the unburnt reactant is initially at T_0 = 900 to 1000 K and P_0 = 10 to 20 atm. As case 3 (T_0 = 900 K, P_0 = 20 atm) indicates, usually only end-gas autoignition and no detonation develops in the corresponding cases with adiabatic walls, where the maximum pressure P_{max} = 106 atm. However, P_{max} reaches 1459 atm in case 3 with an isothermal cold wall. Therefore, the cold isothermal boundary can greatly promote the detonation development and lead to extremely destructive superknock under hydrogen-fueled SI engine relevant conditions.

4. Conclusions

In this work we find that even for hydrogen without NTC behavior, a cold wall can still initiate and promote detonation. The small excitation time and large diffusivity of hydrogen allows this DDT occurring in the very thin thermal boundary layer on the wall. The main conclusions are:

1. The mechanism on detonation from the cold wall is briefly summarized as: great wall heat loss renders autoignition occurring outside the boundary layer instead of on the wall, and then large temperature gradient on the cold wall greatly facilitates DDT of the right branch. Depending on the initial temperature and pressure, the extent of detonation development varies and hence multiple dynamics are involved. Detailed structures, such as post-shock autoignition, shock, reaction front, and detonation are resolved. Corresponding wall interactions are also interpreted.

2. Detonation can also develop from the reaction front. Coupling with the wall-induced detonation, triple detonation waves can be generated, where double shock wave-wall interactions can be observed before the reaction front reaches the wall. However, the combustion mode in the bulk gas is minimally affected by the isothermal boundary when no detonation is generated near the wall.

3. A regime diagram describing different combustion modes is proposed. The boundary of normal combustion can be predicted by the Livengood-Wu integral, whereas the detonation initiation from the wall and reaction front observes the Zel'dovich mechanism. Compared to hydrocarbons, hydrogen is resistant to knock onset but it is more prone to extremely destructive detonation development, which can be promoted by a cold wall.

The present results identify the possibility on superknock initiation for hydrogen/air mixtures due to heat loss at wall. This work provides a first step towards a better understanding of how a transient heat transfer to the cold wall helps the detonation initiation in mixtures without NTC behaviors via Zeldovich mechanism, and thereby a simple 1D configuration is considered. In future works, it would be interesting to consider the role of side wall effects, turbulence mixing and flame instabilities in complex flow configurations.

Acknowledgements

This research was funded by National Natural Science Foundation of China (No. 51861135309). The authors acknowledge helpful discussions with Dr. Pengfei Yang and Dr. Dehai Yu at Peking University.

Supplementary Material

Two Supplementary Material are associated with this article. Supplementary Material 1 shows the numerical treatment of isothermal boundary condition, grid dependence study, and comparison with corresponding adiabatic cases. Supplementary Material 2 provides movies for six demonstrative cases in the simulation.

References

[1] T. Sinigaglia, F. Lewiski, M.E. Santos Martins, and J.C. Mairesse Siluk, Production, storage, fuel stations of hydrogen and its utilization in automotive applications-a review, *International Journal of Hydrogen Energy* 42 (2017) 24597-24611.

[2] S. Verhelst, Recent progress in the use of hydrogen as a fuel for internal combustion engines, *International Journal of Hydrogen Energy* 39 (2014) 1071-1085.

[3] S.E. Hosseini, B. Butler, An overview of development and challenges in hydrogen powered vehicles, *International Journal of Green Energy* 17 (2020) 13-37.

[4] Z. Wang, H. Liu, R.D. Reitz, Knocking combustion in spark-ignition engines, *Progress in Energy and Combustion Science* 61 (2017) 78-112.

[5] Z. Wang, Y. Qi, X. He, J. Wang, S. Shuai, and C.K. Law, Analysis of pre-ignition to super-knock: Hotspot-induced deflagration to detonation, *Fuel* 144 (2015) 222-227.

[6] Y.B. Zeldovich, Regime classification of an exothermic reaction with nonuniform initial conditions, *Combustion and Flame* 39 (1980) 211-214.

[7] Y.B. Zel'dovich, V.B. Librovich, G.M. Makhviladze, and G.I. Sivashinsky, On the development of detonation in a non-uniformly preheated gas, *Astronautica Acta* 15 (1970) 313-321.

[8] J.H. Lee, The Detonation Phenomenon. Cambridge University Press, Cambridge, 2008.

[9] J.H. Lee, R. Knystautas, N. Yoshikawa, Photochemical initiation of gaseous detonations, *Astronautica Acta* 5 (1978) 971-982.

[10] X.J. Gu, D.R. Emerson, D. Bradley, Modes of reaction front propagation from hot spots, *Combustion and Flame* 133 (2003) 63-74.

[11] D. Bradley, C. Morley, X.J. Gu, and D.R. Emerson, Amplified Pressure Waves During Autoignition: Relevance to CAI Engines, *SAE Transactions* 111 (2002) 2679-2690.

[12] M.D. Kurtz, J.D. Regele, Acoustic timescale characterisation of a one-dimensional model hot spot, *Combustion Theory and Modelling* 18 (2014) 532-551.

[13] P. Dai, Z. Chen, S. Chen, and Y. Ju, Numerical experiments on reaction front propagation in n-heptane/air mixture with temperature gradient, *Proceedings of the Combustion Institute* 35 (2015) 3045-3052.

[14] J. Jayachandran, F.N. Egolfopoulos, Thermal and Ludwig–Soret diffusion effects on near-boundary ignition behavior of reacting mixtures, *Proceedings of the Combustion Institute* 36 (2017) 1505-1511.

[15] M.A. L1Berman, V.V. Bychkov, S.M. Golberg, and L.E. Eriksson, Numerical Study of Curved Flames under Confinement, *Combustion Science and Technology* 136 (1998) 221-251.

[16] H. Yu, Z. Chen, End-gas autoignition and detonation development in a closed chamber, *Combustion and Flame* 162 (2015) 4102-4111.

[17] J. Pan, H. Wei, G. Shu, and R. Chen, Effect of pressure wave disturbance on auto-ignition mode transition and knocking intensity under enclosed conditions, *Combustion and Flame* 185 (2017) 63-74.
[18] P. Dai, Z. Chen, X. Gan, and M.A. Liberman, Autoignition and detonation development from a hot spot inside a closed chamber: Effects of end wall reflection, *Proceedings of the Combustion Institute* 38 (2021) 5905-5913.
[19] H. Terashima, M. Koshi, Mechanisms of strong pressure wave generation in end-gas autoignition during knocking combustion, *Combustion and Flame* 162 (2015) 1944-1956.
[20] A. Sow, B.J. Lee, F.E. Hernández Pérez, and H.G. Im, Detonation onset in a thermally stratified constant volume reactor, *Proceedings of the Combustion Institute* 37 (2019) 3529-3536.
[21] C. Wang, Y. Zhao, W. Han, Effect of Heat-Loss Boundary on Flame Acceleration and Deflagration-to-Detonation Transition in Narrow Channels, *Combustion Science and Technology* 189 (2017) 1605 - 1623.
[22] W. Han, J. Huang, G. Gu, C. Wang, and C.K. Law, Surface heat loss and chemical kinetic response in deflagration-to-detonation transition in microchannels, *Physical Review Fluids* 5 (2020) 053201.
[23] M.-H. Wu, C.-Y. Wang, Reaction propagation modes in millimeter-scale tubes for ethylene/oxygen mixtures, *Proceedings of the Combustion Institute* 33 (2011) 2287-2293.
[24] Z. Chen, M.P. Burke, Y. Ju, Effects of Lewis number and ignition energy on the determination of laminar flame speed using propagating spherical flames, *Proceedings of the Combustion Institute* 32 (2009) 1253-1260.
[25] Z. Chen, Effects of radiation and compression on propagating spherical flames of methane/air mixtures near the lean flammability limit, *Combustion and Flame* 157 (2010) 2267-2276.
[26] J. Li, Z. Zhao, A. Kazakov, and F.L. Dryer, An updated comprehensive kinetic model of hydrogen combustion, *International Journal of Chemical Kinetics* 36 (2004) 566-575.
[27] R.J. Kee, G. Dixon-Lewis, J. Warnatz, M.E. Coltrin, and J.A. Miller, A Fortran computer code package for the evaluation of gas-phase multicomponent transport properties, *Sandia National Laboratories Report SAND86-8246* 13 (1986) 80401-1887.
[28] Y. Qi, Z. Wang, J. Wang, and X. He, Effects of thermodynamic conditions on the end gas combustion mode associated with engine knock, *Combustion and Flame* 162 (2015) 4119-4128.
[29] Y. Qi, Y. Wang, Y. Li, J. Wang, X. He, and Z. Wang, Auto-ignition characteristics of end-gas in a rapid compression machine under super-knock conditions, *Combustion and Flame* 205 (2019) 378-388.
[30] Z. Wang, H. Liu, T. Song, Y. Qi, X. He, S. Shuai, and J. Wang, Relationship between super-knock and pre-ignition, *International Journal of Engine Research* 16 (2014) 166-180.
[31] G.T. Kalghatgi, D. Bradley, Pre-ignition and 'super-knock' in turbo-charged spark-ignition engines, *International Journal of Engine Research* 13 (2012) 399-414.
[32] A. De Lataillade, F. Dabireau, B. Cuenot, and T. Poinsot, Flame/wall interaction and maximum wall heat fluxes in diffusion burners, *Proceedings of the Combustion Institute* 29 (2002) 775-779.
[33] T. Poinsot, D. Veynante, Theoretical and numerical combustion. RT Edwards, Inc., 2005, p. 349-373.
[34] C.K. Law, Combustion Physics. Cambridge university press, 2010.
[35] S. Szwaja, J.D. Naber, Dual nature of hydrogen combustion knock, *International Journal of Hydrogen Energy* 38 (2013) 12489-12496.
[36] P. Dai, C. Qi, Z. Chen, Effects of initial temperature on autoignition and detonation development in dimethyl ether/air mixtures with temperature gradient, *Proceedings of the Combustion Institute* 36 (2017) 3643-3650.